Multicomponent 5-fluorouracil loaded PAMAM Stabilized–Silver Nanocomposites Synergistically Induce Apoptosis in Human Cancer Cells

Multicomponent 5-fluorouracil loaded PAMAM Stabilized-Silver Nanocomposites Synergistically Induce Apoptosis in Human Cancer Cells

Ishita Matai[a], Abhay Sachdev[a] and P.Gopinath*[a,b]

[a]Nanobiotechnology Laboratory, Centre for Nanotechnology,
[b]Department of Biotechnology,
Indian Institute of Technology Roorkee, Roorkee, Uttarakhand-247667, India.
Fax: +91-1332-273560;
Tel: 91-1332-285650;
E-mail: pgopifnt@iitr.ernet.in, genegopi@gmail.com

Abstract

Herein, we report development of poly (amidoamine) (PAMAM) dendrimer based multicomponent therapeutic agent for *in vitro* cancer therapy applications. In this approach, Generation 5 (G5) PAMAM dendrimers stabilizing silver nanoparticle surface (DsAgNPs) were used to encapsulate anticancer drug 5-fluorouracil (5-FU) to attain synergism in cancer cells. 5-FU loaded DsAg nanocomposites (5-FU@DsAgNCs) were characterized by UV-visible spectroscopy, transmission electron microscopy, X-ray diffraction and nuclear magnetic resonance measurements. *In vitro* release studies certify the sustained release of 5-FU from nanocomposites. 5-FU@DsAgNCs were found to elicit synergistic antiproliferative effect in A549 (Human lung cancer) and MCF-7 (Human breast cancer) cells with IC_{50} 5 µg mL^{-1} and 1.5 µg mL^1, and combination index (CI) values of 0.242 and 0.178, respectively. Atomic absorption spectroscopic analyses indicated higher cellular uptake of Ag in MCF-7 than A549 cancer cells. Nuclear and morphological alterations, typical of apoptosis induction were revealed by fluorescence and scanning electron microscope imaging. Increment in reactive oxygen species (ROS) levels was measured which indicated induction of oxidative stress in 5-FU@DsAgNC treated both cell types. Taken together, the apoptotic effects of 5-FU@DsAgNC were more prominent in MCF-7 than A549 cancer cells. Finally, gene expression studies suggested triggering of p53 mediated caspase signalling gene cascade in 5-

FU@DsAgNC treated cells. The strategy to use dendrimer technology to design multicomponent 5-FU@DsAgNCs is quite promising for simultaneous delivery of 5-FU and DsAgNPs to achieve synergistic anticancer effects.

Keywords: PAMAM dendrimer, AgNPs, 5-FU, Apoptosis, Cancer therapy.

1. Introduction

Lung cancer is the most recurrent cause of cancer-related deaths worldwide followed by breast cancer. [1] Till date, chemotherapy is the most evolved treatment for cancer which relies on administration of bolus doses of drugs systemically to cancer patients. [2] However, development of multidrug resistance in cancer cells in response to chemotherapy is a major obstacle which restrains the effective drug accumulation. Combinatorial therapy including multiple drugs or potential drug candidates with distinct signalling pathways, enhanced therapeutic effects against specific targets and routes to overcome mechanisms of resistance is a promising alternative to single-agent chemotherapy.[3] In this regard, nanotechnology mediated delivery of anticancer agents under a single therapeutic platform can prove to be an effective strategy.

Over the past few decades, polymer based nanoscale drug delivery systems (DDS) as 'nanomedicines' have garnered much attention for the chemotherapeutic drug delivery in cancer treatment. With suitable design and structural versatility, they provide biocompatibility, controlled drug release profiles, increased circulation times and accumulation at tumor site as a result of enhanced permeability and retention (EPR) effect. [4-6] Such advantages suggest the pre-eminence of nanoscale drug carriers over traditional drugs. Among the available polymers, dendrimers especially PAMAM dendrimers offer numerous advantages which include (i) monodispersity, (ii) enhanced solubility of

hydrophobic drugs, (iii) reduced toxicity compared to free drugs, (iv) tumor selectivity by EPR effect, and (v) can bypass p-glycoprotein-mediated drug resistance.[5,7,8] PAMAM dendrimers with hydrophobic cavities have been known for encapsulation and delivery of hydrophobic anticancer drugs such as 5-fluorouracil (5-FU) [9,10], doxorubicin [11,12], paclitaxel [13,14] , curcumin [15,16] etc. The solubility enhancement property of dendrimers make them an excellent choice as a cargo for insoluble anticancer drugs. [17]

In addition, pertinence of amine terminated PAMAM dendrimers as templates or stabilizers for metal nanoparticle synthesis have been reported. [18-20] High generation PAMAM dendrimers comprising of abundant terminal amines and amide linkages are contemplated to reduce and stabilize metal nanoparticles. Many groups have reported the role of G5 PAMAM dendrimer terminal groups in formation of dendrimer entrapped /stabilized gold and silver nanoparticles. [19,20] Use of G5 PAMAM dendrimer stabilized gold, silver and gold-silver alloy nanoparticles as potential computed tomography (CT) imaging agents have been reported. [21-23] However, use of such PAMAM based metal nanoparticles as drug carriers for cancer therapeutics is not yet studied. Pre-existing literature suggests the use of silver nanoparticles (AgNPs) as apoptosis (programmed cell death) inducing agents. [24-28] Moreover, 5-FU is an established cytotoxic drug used in the treatment of lung, breast, skin, liver, colon, bladder, pancreatic, head and neck cancers. [29] 5-FU is known to inhibit the activity of thymidine synthetase (TS) enzyme involved in DNA synthesis and arrests cell growth. However, its limited tissue and cell biodistribution profiles with side effects in form of liver damage and digestive discomfort limits its usage. [30] 5-FU has been used in conjunction with anticancer drugs, such as curcumin, cisplatin as well as nanoparticles of silver and selenium to exhibit synergistic anticancer effects. [31-33, 29] In addition, some groups have shown the anticancer potential of 5-FU loaded PAMAM dendrimers *in vitro*. Tran and

co-workers demonstrated the antiproliferative activity of 5-FU grafted Pegylated PAMAM dendrimers (G3) against MCF-7 (breast cancer) cells and obtained IC_{50} of 9.92 ± 0.19 μg mL^{-1}.[9] Mei and group studied the inhibitory effects of 5-FU PAMAM dendrimer in combination with antisense micro-RNA 21 gene therapy to enhance the chemo sensitivity of 5-FU in MCF-7 cells.[10] However, the strategy to combine nanoparticles and anticancer drugs with different action mechanisms within PAMAM based carriers still remains unexplored.

The present study introduces a new dimension wherein, dual functionality of PAMAM dendrimer, as a stabilizer for amine terminated AgNPs and carrier for 5-FU for cancer therapy has been exploited. Combinatorial therapy of AgNPs and 5-FU drug in a single PAMAM nanocarrier enable their co-delivery in sufficient amounts to cancer cells *in vitro* for attaining synergistic anticancer effects. To the best of our knowledge, this is the first instance employing dual functionality of PAMAM dendrimer as a stabilizer and a drug carrier to further investigate it's *in vitro* anticancer effects. The rationale behind is to kill the cancer cells by combination of two separate mechanistic pathways: caspase activation pathway and reactive oxygen species (ROS) induction for efficient apoptosis. We have tested the ability of 5-FU loaded dendrimer stabilized silver nanocomposites (5-FU@DsAgNCs) to induce apoptosis in human lung and breast adenocarcinoma cell lines i.e. A549 and MCF-7. Interestingly, MCF-7 cells were found to be more susceptible to 5-FU@DsAgNC treatment than A549 cells.

2. Experimental Section

2.1. Materials and Methods

Ethylenediamine core G5.NH$_2$ PAMAM dendrimer (Molecular weight 28824.81 g/mol) and 5-FU (purity > 99%) were purchased from Sigma-Aldrich. Methanol content in dendrimer

solution was removed by rotary evaporation under reduced pressure. Silver nitrate and sodium borohydride were purchased from Merck (Germany). All the preparations were done in ultrapure water at room temperature in dark colored vials.

2.2. Synthesis of G5 PAMAM dendrimer stabilized silver nanoparticles (DsAgNPs)

Dendrimer stabilized silver nanoparticles were synthesized as previously reported with slight modification. [18, 20] Briefly, aqueous solution of $AgNO_3$ (2.8 mg, 125 μL) was added to aqueous solution of PAMAM (8.31 mg, 500 μL) under vigorous magnetic stirring (@ 660 rpm). After 30 min, 200 μL of ice cold $NaBH_4$ sol. (2.2 mg, water/methanol (v/v 3:1)) was added to the above mixture and the reaction was continued for 2 h in dark. The colour of the solution immediately turned dark yellow upon $NaBH_4$ addition. The reaction mixture was then extensively dialyzed using a regenerated cellulose membrane (MWCO 10000 Da) against PBS (3 times, 4L) and water (6 times, 4L) for 3 days to remove excess reactants. The solution was further lyophilized and diluted in appropriate concentration for further drug loading experiments. Concentration of Ag was subsequently determined by inductively coupled plasma mass spectrometry (ICP-MS).

2.3. Preparation of 5-FU loaded DsAg nanocomposites (5-FU@DsAgNCs)

Aqueous solution of 5-FU and DsAgNPs were mixed in 100:1 molar ratio and magnetically stirred (@100 rpm) for 24 h using teflon beads. Free 5-FU was removed by dialysis (MWCO 10000 Da) against water twice under strict sink conditions for 20 min. 5-FU@DsAgNC were then obtained by lyophilization and stored at 4°C for further characterization. Likewise, 5-FU loaded PAMAM (5-FU-D) were synthesized as controls. A standard curve of 5-FU in PBS was generated (0-50 μg mL^{-1}; r^2 = 0.999) using a spectrophotometer and its concentration

inside the complexes was determined by UV absorption at 265 nm. Drug loading efficiency (DLE, wt. %) of 5-FU in 5-FU@DsAgNCs was calculated according to following formula:

DLE (%) = [(Amount of loaded 5-FU/Amount of initial 5-FU)] * 100

2.4. Characterization Techniques

UV-vis spectra were collected with Lasany double-beam L1 2800 UV–Visible spectrometer. Samples were dissolved in water before the experiments. Transmission electron microscopic (TEM) experiments were performed with FEI TECHNAI G2 analytical electron microscope operating at 200 KV. 20 μL of an aqueous solution of dendrimer stabilized AgNPs (1 mg ml^{-1}) was dropped onto a carbon coated copper grid and subsequently air dried before measurements. Size distribution histogram of these amine terminated AgNPs was analysed with ImageJ (http://rsb.info.nih.gov/ij/download.html). 5-FU@DsAgNCs were viewed after negative staining with 2% phosphotungstenic acid (PTA). X-Ray diffraction specta (XRD) were recorded using a Bruker AXS D8 advance powder X-ray diffractometer (Cu-Kα radiation, λ= 1.5406A°) in the range of 20–80∘ at a scan speed of 0.05°/min. Zeta potential (ζ) measurements of PAMAM complexes were determined using Malvern Zetasizer Nano ZS90. ^{1}H NMR spectra of samples were recorded on a Bruker 500 MHz nuclear magnetic resonance (NMR) spectrometer. PAMAM.NH$_2$ complexes were dissolved in D$_2$O in millimolar concentrations before experiments. Elemental mapping was performed using QUANTA 200-FEG electron microscope (FE-SEM) operating at 15 KV. Fluorescence microscopic images of cells were acquired using EVOS FL Color, AMEFC 4300) microscope using DAPI (excitation 360 nm, emission 447 nm), GFP (excitation 470 nm, emission 525 nm) and RFP (excitation 530 nm, emission 593 nm) light cubes, respectively.

2.5. *In Vitro* Release of 5-FU

In Vitro release studies were performed using dialysis bag method. [34] 5-FU@DsAgNCs were prepared with a 5-FU concentration of 0.4 mg mL^{-1}. 3 mL of sample solution was placed in a dialysis bag (MWCO 10000), hermitically tied and placed in 200 mL PBS (pH 7.4) at 37˚C with mild agitation (70 rpm). Subsequently, 1.0 mL of dissolution medium was withdrawn at specific time intervals up to 48 h and replaced with same volume of fresh PBS. Pure 5-FU in water at an equivalent concentration was applied as control to monitor its permeation through dialysis bag. The cumulative 5-FU release was determined by measuring absorbance at 265 nm using calibration curve. % release was calculated as:

% Release = [(Conc. of drug $_{aliquot}$ * Volume of release medium)/Initial drug conc.] * 100

2.6. Cell Culture

A549 and MCF-7 (human lung and breast adenocarcinoma cell lines, NCCS Pune) were cultured in Dulbecco's modified Eagle's medium (DMEM) comprising of 10% fetal bovine serum (FBS) supplemented with 1% penicillin-streptomycin and maintained at 37°C in a humidified incubator with 5% CO_2 atmosphere. Cells were subcultured every 48 h and harvested from subconfluent cultures (60-70%) using 0.25% trypsin-EDTA.

2.7. MTT Assay

Cytotoxicity was evaluated by MTT, a mitochondrial based cell viability assay. Cell viability was assessed on the ability of cells to transform tetrazolium salt to purple formazon crystals. A549 and MCF-7 cells at a density of 10^4 cells/well were seeded in 96 well plate (Corning, Costar, NY) and were allowed to attach overnight. The cells were then exposed to different concentrations of G5 PAMAM dendrimer, 5-FU-D, DsAgNPs and 5-FU@DsAgNCs for 48

h. After exposure, medium with PAMAM complexes was removed and PBS wash was given twice. Fresh 100 μL DMEM medium with MTT dye (5 mg mL^{-1}) was added per well and cells were incubated for another 4 h. To dissolve the formazon crystals formed medium was aspirated and 100 μL of lysis solution was added. By measuring the color intensity of formazon solution we can estimate the cell growth condition or cell viability. The soluble formazon product was measured using multimode reader (Cytation3, Biotek) at 570 nm and the background control at 690 nm. Cell Viability (%) was calculated as:

% Cell viability = [(A$_{570}$- A$_{690}$) treated/ (A$_{570}$- A$_{690}$) control] * 100.

2.8. Synergy Analysis and Combination Index (CI) Value Determination

The synergistic inhibitory effect of 5-FU and AgNPs loaded in the PAMAM nanocarrier was evaluated by the isobologram method. [35] Briefly, a straight line was formed by plotting the IC$_{50}$ value of 5-FU-D and DsAgNPs on the x- and y- axes, respectively. The data point in the isobologram correspond to the actual IC$_{50}$ value of 5-FU@DsAgNCs. If the data point lies on or near to the line, it indicates additive treatment effect, whereas the position of data point below or above the line suggests synergism or antagonism, respectively. Moreover, CI value was also determined to examine the interaction between the two components by Chou Talalay's method. [36] CI is a dimensionless quantity and a CI value of 1, <1 or >1 indicates additive, synergistic or antagonistic effect, respectively. For an effective treatment, synergism reflected by a CI value < 1 is desirable.

2.9. *In Vitro* Cellular Uptake Studies

Quantitative estimation of uptake of Ag by A549 and MCF-7 cells was done by atomic absorption spectroscopy (AAS) in the graphite furnace mode (Avanta M, GBC). A549 and

MCF-7 cells were seeded separately in a 6-well plate ($2x10^5$ cells/well) for overnight attachment. Cells were then exposed to different concentrations of 5-FU@DsAgNCs (2.5, 5 μg mL^{-1} Ag equivalent) for 3 h. After exposure, cells were thoroughly washed to remove the unbound Ag, harvested and counted. 1 mL of 0.5% triton X-100 in 0.2 N NaOH solution was added to lyse the cells completely. Samples were further acidified with 65 wt. % HNO_3 to ensure complete digestion of Ag complexes before measurement. Parallel blanks (untreated cells) were set to calculate the net cellular uptake. Results were expressed in form of cellular dose i.e. mean amount of Ag in pg/cell. [24]

2.10. Acridine Orange /Ethidium Bromide (AO/EB) Dual Staining

Apoptotic effects of 5-FU@DsAgNCs against A549 and MCF-7 cells was examined by AO/EB staining. [26] Briefly, $2x10^5$ cells/well seeded in a 6-well tissue culture plate and were allowed to attach overnight. Cells were then exposed to different concentrations of 5-FU@DsAgNCs for around 24 h. Following treatment, ice cold PBS wash was given and cells were incubated with AO/EB (10 μg mL^{-1} working concentration) at 37°C for 15 min. Subsequently, once PBS wash given to remove excessive dyes. Images were captured under different filters using EVOS cell imaging system (life technologies, USA).

2.11. Cell Morphology Analysis and Elemental Mapping by FE-SEM

A549 and MCF-7 cells were grown on sterile glass coverslips and were then treated with IC$_{50}$ concentration (by MTT assay) of 5-FU@DsAgNCs for 24 h. Cells were then fixed with 2% glutaraldehyde for 10 min followed by ethanol gradient fixation (20%, 40%, 60%, and 80%). Cell membrane integrity of air dried samples was then examined by FE-SEM. Further, elemental mapping was done to verify the elemental distribution of 5-FU and Ag in 5-FU@DsAgNC treated cells.

2.12. Time Dependent Morphological Examination

Nuclear chromatin compaction and alteration in cytoskeleton can be assessed with a combination of fluorescent dyes-Hoechst 33342 and rhodamine B (Rho B). MCF-7 and A549 cells ($2x10^5$ cells/well) seeded in a 6-well plate were treated with 5-FU@DsAgNCs for 6, 12, 24 h. Following treatment, DMEM medium was removed and mild PBS wash was given to remove dead floating cells. Cells were then incubated with 2 μL Hoechst dye (10 mg mL^{-1}) and 5 μL Rho B (1 mg mL^{-1}) for 10 -15 min at 37˚C. An overlay of images acquired under DAPI and red filters was taken.

2.13. Intracellular ROS Generation

MCF-7 and A549 cells grown in 6 well plate were treated with appropriate concentrations of 5-FU@DsAgNCs for 3 h. Cells were then supplemented with 1 mL fresh DMEM containing 20 μM 2,7-dichlorofluorescin diacetate (DCFH-DA ,Sigma Aldrich) dye and incubated for 10 min at 37°C. Following incubation, cells were harvested and resuspended in PBS. DCFH-DA is a cell permeant fluorogenic dye used to measure ROS activity within the cell. Upon cellular diffusion, cleavage of the acetate groups by intracellular esterases occurs and DCFH-DA is converted to the highly fluorescent 2, 7-dichlorofluorescein (DCF) upon oxidation. [24, 25] DCF has an excitation and emission maxima at 495 nm and 529 nm, respectively. Immediately after incubation, samples were analyzed for DCF fluorescence using flow cytometer (Amnis Flowsight). Amnis Ideas software was used to analyze the acquired data for 10000 events per sample and ROS generation was expressed in terms of percentage of cells with green (DCF) fluorescence.

2.14. Gene Expression Studies

Differential expression of apoptotic signaling genes when exposed to 5-FU@DsAgNCs was detected using semi-quantitative reverse transcriptase- polymerase chain reaction (RT-PCR). Beta-actin (housekeeping gene) was used as an internal control. Total RNA was extracted from MCF-7 cells using Tri reagent (Sigma Aldrich, USA) and cDNA was generated by reverse transcription of 1 µg of denatured RNA. The forward and reverse primer sequences used are mentioned in Table S1 (Supporting information). Cycle steps involved an initial denaturation at 94°C for 3min followed by PCR cycle of denaturation at 94°C for 30s, annealing at 60°C for 30s, extension at 72°C for 1min with a final extension at 72°C for 10min. The PCR products were finally resolved in 1% agarose gel and visualized by ethidium bromide staining under UV light. Image lab 4.0 software was used to compute the fold difference.

2.15. Statistical Analysis

The values are expressed as mean ± S.E.M for individual experiments. The data were analyzed by Student's *t* test or by two-way ANOVA whichever applicable, using GraphPad Prism 6.0 and statistically significant values are denoted by ∗ ($p < 0.05$), ∗∗ ($p < 0.005$), and ∗∗∗ ($p < 0.001$).

3. Results and Discussion

3.1 Synthesis and Characterization of 5-FU@DsAgNCs

The objective of this work is to construct a PAMAM based therapeutic agent wherein it serves the dual role of a stabilizer for silver nanoparticles and as a delivery system for anticancer drug 5-FU. To achieve this, dendrimer stabilized AgNPs were synthesized using dendrimer terminal amine/Ag salt molar ratio 100:1 and $NaBH_4$ reduction to obtain one

AgNP stabilized by multiple dendrimers. [18] Next step was to entrap partially insoluble drug 5-FU in the internal PAMAM cavities. The interactions responsible in 5-FU-PAMAM dendrimer complexation include (i) mainly hydrogen bond formation, (ii) weaker hydrophilic interactions (with polar internal PAMAM groups – tertiary amine and amide) and (iii) much weaker hydrophobic interactions. [37] **(Scheme S1, Supporting Information)**

UV-vis spectrometry was first used to qualitatively confirm the formation of amine terminated AgNPs and successful loading of 5-FU in the PAMAM G5 interiors **(Figure 1a).** Appearance of two absorption peaks in 5-FU@DsAgNCs (black line): one at 410 nm is attributed to typical surface plasmon resonance (SPR) band of AgNPs [20, 22] while the other at 266 nm is the typical absorption peak of 5-FU. [10] In contrast, amine terminated AgNPs (red line) display only one peak at 419 nm corresponding to SPR band of AgNPs. Inset in **Figure 1a** shows photographs of pure G5 PAMAM dendrimer (colorless, 1), DsAgNPs (yellow, 2) and 5-FU@DsAgNCs (golden yellow, 3). The transition in color confirms the formation of 5-FU@DsAgNCs.

The concentration of Ag in the PAMAM complexes estimated by ICP-MS was 175 µg mL^{-1}. Drug loading efficiency (DLE, wt. %) of 5-FU in 5-FU@DsAgNCs estimated from the standard curve ($y = 0.047x + 0.02$; r^2 0.999) was 25.9 ± 3.5 % i.e. around 26 molecules of 5-FU were loaded per dendrimer. This is in accordance with the previous findings of Buczkowski et al., 2012. [37]

Further, TEM analysis was done to characterize the formed DsAgNPs and 5-FU@DsAgNCs. It was clear that the formed DsAgNPs were spherical in shape with an average size distribution of 8.32 nm (± 1.13 nm) much bigger than the PAMAM G5 size (5.4 nm)

indicating formation of dendrimer stabilized AgNPs and not entrapped nanoparticles **(Figure 1b)**. Size distribution histogram of DsAgNPs is shown in **Figure S1 (Supporting Information)**. Negative staining with PTA enabled view of homogenous distribution of DsAgNPs loaded with 5-FU **(Figure 1c)** and its corresponding selected area diffraction pattern (SAED) is depicted in **Figure 1d.** Bright spots in SAED pattern are ascribed to crystalline silver with phases (111), (200), (220) and (311). 5-FU did not contribute to the SAED pattern which recommend its complete encapsulation in the dendrimer interiors. Energy dispersive spectroscopy (EDS) confirmed the existence of Ag and F (of 5-FU) elements in the 5-FU@DsAgNCs **(Figure S2, Supporting Information).** Structural characteristics of 5-FU@DsAgNCs were further interpreted by XRD and match with the above SAED findings **(Figure S3, Supporting Information).** Appearance of crystallographic phases (111), (200), (220) and (311) in 5-FU@DsAgNCs confirm the formation of crystalline face centered cubic Ag. [38] No separate peaks of 5-FU were identified which confirms its complete encapsulation.

Accounting the stability of 5-FU@DsAgNCs under physiological conditions is of utmost importance for their biological applications. 5-FU@DsAgNCs in powder form were readily soluble in water and PBS with appreciable stability for at least 2 months at 4°C. Changes in the surface charge potential with 5-FU encapsulation were recorded **(Figure S4, Supporting Information)**. As seen, Zeta potential (ζ) of G5 PAMAM was +49.6 mV which decreased to +44 mV with formation of dendrimer stabilized Ag. The slight reduction in charge can be ascribed to utilization of few terminal NH_2 groups for stabilizing the nanoparticle surface. Surprisingly, the ζ values increased to +45.6 mV with 5-FU encapsulation, explaining higher stability of 5-FU@DsAgNCs than DsAg. Liu et al., 2012 obtained similar results for 5-FU-

SeNPs where surface decoration of 5-FU increased the stability of SeNPs. [29] The high

stability of 5-FU@DsAgNCs is essential for their future biomedical applications.

3.2. ^{1}H NMR Analysis

The formation of DsAgNPs and 5-FU@DsAgNCs was further confirmed by ^{1}H NMR

measurements. **Figure 2** represents the ^{1}H NMR spectra of PAMAM.NH$_2$, DsAgNPs and 5-

FU@DsAgNCs. Significant difference in the chemical shift of protons related to DsAgNPs

(Figure 2b) and 5-FU@DsAgNCs **(Figure 2c)** were observed compared to G5

PAMAM.NH$_2$ dendrimers **(Figure 2a)**. Upon formation of DsAg, ^{1}H NMR signals related to

4, 5, 6 protons of G5 PAMAM.NH$_2$ dendrimers shift downfield while remaining protons

retain their original position. This signifies the interaction of dendrimer secondary and

terminal amines with the surface of Ag nanoparticle. [19] These interactions are predominantly

involved in formation of amine terminated AgNPs. With 5-FU entrapment, only protons 1

and 3 of G5 PAMAM.NH$_2$ demonstrated a downfield chemical shift when compared to DsAg

while the position of other protons remained unchanged. This presumably is due to strong

complexation between secondary amines and amide groups with the 5-FU drug. [39]

3.3. *In Vitro* 5-FU Release Kinetics

Before moving to cellular environments we investigated the ability of PAMAM dendrimers

to release the 5-FU payload under physiological conditions. **Figure 3a** shows the release

profiles of free 5-FU and 5-FU from 5-FU@DsAgNCs in PBS (pH 7.4).It can be seen that

cumulative release of 5-FU from NCs was in a sustained manner. In contrast, about 90% free

5-FU was released within 6h while less than 30% 5-FU released from 5-FU@DsAgNCs in

the same time period. These nanocomposites were able to release 5-FU in a biphasic pattern,

characterized by an initial faster release followed by a sustained release. [11, 12] The initial

burst release can be owed to diffusion of loosely bound 5-FU molecules in the dendrimer interiors or 5-FU adsorbed on the nanoparticle surface. **Figure 3b** represents the schematic representation of the diffusion of bound 5-FU drug molecules from the dendrimer hydrophobic interiors with exposure to physiological environment.

3.4. Investigation of Growth Inhibition by 5-FU@DsAgNCs

3.4.1 In Vitro Cytotoxicity Assay

The *in vitro* cytotoxicity of 5-FU@DsAgNCs was tested against A549 and MCF-7 cancer cells by MTT assay. Drug 5-FU and AgNPs as constituting elements of PAMAM nanocomposites exhibited growth inhibition in a dose-dependent manner **(Figure 4).** 5-FU@DsAgNCs synergistically induced cell death at far less dosage compared to DsAgNPs and 5-FU-D complexes in both cell lines. The half maximum inhibitory concentration (IC_{50}) of 5-FU@DsAgNCs recorded against A549 and MCF-7 was found to be 5 µg mL^{-1} and 1.5 µg mL^{-1}, respectively. However, PAMAM dendrimer showed minimal toxicity up to 20 µg mL^{-1} which indicate that the cell death was primarily due to combined action of 5-FU and AgNPs. Interestingly, cytotoxic effects of 5-FU@DsAgNCs were more pronounced in MCF-7 than A549 cells. These results indicate that the synergistic effects of 5-FU@DsAgNCs are cell-type specific. The selectivity in action could be attributed to different gene expression profiles of MCF-7 and A549 cells, involved in activation of different intracellular signalling pathways. [29]

3.4.2 Isobologram Analysis

The synergistic interaction between DsAgNPs and loaded drug (5-FU) was studied by isobologram examination. The IC_{50} values for 5-FU@DsAgNCs, DsAgNPs and 5-FU-D were found at 5, 15 and 30 µg mL^{-1} for A549 and 1.5, 5 and 20 µg mL^{-1} for MCF-7, respectively.

Isobologram analysis revealed that viability inhibition of combined 5-FU and DsAgNPs treatment was strongly synergistic, as evidenced from the location of data point in isobologram being far below the additive line **(Figure 4c, d).** The combination index (CI) of the IC_{50} value of 5-FU@DsAgNCs was calculated as 0.242 (for A549) and 0.178 (for MCF-7) which confirms the synergistic interaction between 5-FU and DsAgNPs. [35] Collectively, our results clearly demonstrate that the strategy to combine 5-FU with DsAgNPs can effectively augment its anticancer potential.

3.5. Quantification of Cellular Uptake of Ag by AAS

AAS was used to quantify the cellular uptake of silver in both A549 and MCF-7 cells treated with 5-FU@DsAgNCs for 3 h **(Figure S5, Supporting Information).** Cellular uptake of Ag was found to increase in a concentration dependent manner for both the cell types. The results indicate that at the studied Ag concentrations, the amount of Ag uptake in MCF-7 is significantly higher than in A549 cells. Presumably more uptake of Ag or 5-FU@DsAgNCs in MCF-7 cells, can be held responsible for its higher cytotoxicity than A549 cells.

3.6. Induction of Apoptosis in Cancer cells

AO/EB staining, FE-SEM and Nuclear Fragmentation Studies

Apoptosis has been proposed as the main mechanism of anticancer action of 5-FU [31, 40] and Ag. [41, 42] So, in order to determine the mode of cancer cell death (viz. apoptosis or necrosis) by 5-FU@DsAgNCs, treated cells were stained with fluorescent DNA intercalating dyes namely AO/EB and observed under fluorescence microscope. AO dye can permeate all cell nucleus to emit green fluorescence on binding with double stranded DNA but EB can only enter the membrane compromised nucleus to emit orange-red fluorescence. [26] As evident from **Figure 5a**, IC_{50} treated A549 and MCF-7 cells showed green and orange-stained

condensed nuclei owing to both early and late apoptotic cells. While 2X IC$_{50}$ treated cells, displayed more number of late apoptotic cells and few necrotic cells. Thus, AO/EB staining signify apoptosis induction by 5-FU@DsAgNCs in both cancer cell types.

We next performed FE-SEM studies to monitor cell morphological changes associated with apoptosis. As seen in **Figure 5b**, untreated cells have distinct shape and are well attached to the surface with no evidence of membrane constriction or leakage. Contrarily, IC$_{50}$ treated cells were spherical and loosely-bound. Membrane blebbing and formation of apoptotic bodies, characteristics of apoptotic cell death [43], were clearly evident in 5-FU@DsAgNC treated cells. Following, elemental mapping detected the distribution profiles of elements, F (of 5-FU) and Ag in treated MCF-7 cells which verifies the apoptosis inducing ability of 5-FU@DsAgNCs **(Figure S6, Supporting Information).**

Besides membrane blebbing, nuclear chromatin condensation and cytoplasmic shrinkage are key features of apoptotic cells. [44-46] In this regard, time dependent induction of apoptosis in form of nuclear fragmentation and cytoskeleton compaction was studied at three time points i.e. at 6, 12 and 24 h using Hoechst 33342 and rho B dyes. Basically, Hoechst 33342 is a membrane permeant nuclear counterstain that emits blue fluorescence when bound to dsDNA. It can differentiate condensed pycnotic nuclei (nucleus with condensed chromatin) in apoptotic cells [47], while rho B stains the mitochondria and cytoplasmic compartments. [31]

In the present case, as evident in **Figure 6**, with time course 5-FU@DsAgNC (IC$_{50}$) treated MCF-7 nuclei exhibited chromatin condensation in form of dark spots (marked with yellow arrows) and a significant reduction in cytoplasmic volume (white arrows). After 24 h, drastic reduction in cell number with very few rho B stained cells and appearance of many pycnotic

nuclei suggest MCF-7 apoptotic cell death. Similar were the observations with 5-FU@DsAgNC (IC$_{50}$) treated A549 cells **(Figure S7, Supporting Information)**.Taken together, these findings suggest that cell death induced by 5-FU@DsAgNCs is mainly caused by apoptosis.

3.7. 5-FU@DsAgNCs Induce Oxidative Stress by Evoking ROS

Oxidative stress has been considered as one of the most crucial mechanisms of toxicity upon Ag nanoparticle exposure. [41, 42] Excessive generation of ROS result in disturbance of cells intrinsic antioxidant defence mechanisms and induction of oxidative stress. This oxidative stress causes mitochondrial dysfunction, DNA damage and finally apoptotic cell death. [25,26] To evaluate the potential role of oxidative stress mediated by 5-FU@DsAgNC exposure, ROS levels were measured using DCFH-DA assay. In MCF-7 cells, the percentage of ROS producing cells was 3.88% in untreated cells which increased to 32.7% (~8.5 times) in 1.5 µg mL^{-1} (IC$_{50}$) and to 41.1% (~10.5 times) in 3 µg mL^{-1} (2X IC$_{50}$) treated cells **(Figure 7)**. Comparatively, in A549 cells, % population with ROS induction elevated from 2.48% in untreated cells to 6.58% (~2.5 times) in 5 µg mL^{-1} (IC$_{50}$) and to 19.9% (~8 times) in 10 µg mL^{-1} (2X IC$_{50}$) treated cells **(Figure S8, Supporting Information)**. Complementarily, fluorescent images showed a subsequent increase in number of cells with DCF fluorescence (green) with increase in 5-FU@DsAgNC dose for both MCF-7 and A549 cells **(Figure 7, S8)**. These results suggest that 5-FU@DsAgNCs induced oxidative stress by evoking more ROS in MCF-7 than A549. Moreover, these findings match closely with the MTT results wherein MCF-7 cells were found to be more susceptible to 5-FU@DsAgNC treatment than A549 cells. Hence, MCF-7 cells were selected for elucidating the apoptotic gene expression induced by 5-FU@DsAgNCs.

3.8. 5-FU@DsAgNC Treatment Turns on p53 Mediated Gene Signalling Cascade

RT-PCR analysis of 5-FU@DsAgNC (IC_{50}) treated and untreated MCF-7 cells was done to monitor the expression profiles of pro-apoptotic: p53, caspase 3, c myc, bax, bad and anti-apoptotic: bcl-xl, bcl-2 and β-actin (housekeeping) genes. The results indicated differential expression of various apoptotic genes **(Figure 8a)**. Interestingly, it was observed that pro-apoptotic genes were up-regulated (depicted in figure by upward arrow) and anti-apoptotic genes were down-regulated (depicted in figure by downward arrow). Expression of β-actin remained unaltered. The fold difference in gene expression has been shown in **Figure 8b**.

A schematic illustration of apoptotic pathway involved in 5-FU@DsAgNC treatment is represented in **Figure 8c**. 5-FU@DsAgNC attachment causes membrane destabilization and ROS induction which activates intracellular signalling pathway and triggers activation of p53. Moreover, p53 is also considered as the main effector molecule involved in 5-FU toxicity. [40, 48] 5-FU, principally acts as a thymidylate synthase (TS) inhibitor, an enzyme required for DNA replication and inhibits DNA synthesis. Herein, we have observed up-regulation of p53 gene which indicate activation of p53 mediated signalling cascade. Anti-apoptotic bcl-2 (basal cell lymphoma 2) and bcl-xl (basal cell lymphoma-extra large) protects the cell from undergoing apoptosis and bad (bcl-2-associated death promoter) promotes apoptosis. [49, 50] We observed, down-regulation of bcl-2 and bcl-xl with up- regulation of bad which suggest initiation of apoptosis. Further, p53 is known to up-regulate bax (bcl-2-associated X protein). [51] An elevation in bax expression was seen which postulates the role of p53 in bax up-regulation upon 5-FU@DsAgNC treatment. Translocation of bax from cytosol to mitochondria has been associated with outer membrane permeabilization (MOMP) and formation of pores which allow cytochrome c release. [51] The released cytochrome c is

identified to trigger caspase 3 (cysteine-aspartic acid proteases), the final executioners to apoptosis which cause cellular DNA fragmentation and subsequently cell death.[52, 53] We have observed increased expression of caspase 3 which prompt caspase 3 mediated apoptosis in 5-FU@DsAgNC treated cells. Consecutively, up-regulation of C-myc, a known inducer of apoptosis, promotes apoptotic genes and down-regulates anti-apoptotic genes, bcl-2 and bcl-xl validating manifestation of cell blebbing and p53 mediated apoptotic cell death. Similar results have been reported by Gopinath et al., 2008 [28] and Hsin et al., 2008. [54] Such an understanding of the molecular underpinnings of 5-FU@DsAgNCs mediated cell death can primarily establish 5-FU@DsAgNCs as a potent anticancer weapon to prevent multidrug resistance and cancer recurrence.

4. Conclusion

Our present work describes the construction of a novel G5 PAMAM dendrimer based multicomponent system for simultaneous delivery of AgNPs and anticancer drug 5-FU to cancer cells. Drug 5-FU confined within dendrimer stabilized AgNPs interiors circumvent the limitations associated with multidrug resistance in cancer cells at less dosage to emerge as a potential alternative to traditional chemotherapy. Initially, PAMAM dendrimer stabilized AgNPs were synthesized at dendrimer terminal amine: $AgNO_3$ molar ratio (100:1). Further, chemotherapeutic drug 5-FU was entrapped in the interiors of DsAgNPs. *In vitro* drug release kinetic studies explained the ability of DsAgNPs as a carrier to release the drug cargo i.e. 5-FU under physiological conditions. Further, antiproliferative activity of 5-FU@DsAgNC was assessed on A549 and MCF-7 cancer cell lines. Cytotoxicity studies and isobologram analysis revealed that 5-FU@DsAgNC was able to inhibit the cell growth synergistically. Additionally, 5-FU@DsAgNC treatment generated ROS leading to oxidative stress, augmented DNA condensation and cytoskeleton compaction eventually causing membrane

blebbing and cell injury. Furthermore, 5-FU@DsAgNCs mediated apoptosis, was found an interplay of ROS generation and caspase-signalling pathways. In a nutshell, our results strongly suggest that the strategy to use DsAgNPs as a nanocarrier of 5-FU could be a highly proficient way to achieve synergistic treatment of cancers. Further studies on conjugation of cancer-specific markers onto PAMAM surface for targeted delivery to cancer cells and subsequent modification of external surface to minimize any side effects are underway.

Acknowledgement

References

1. American Cancer Society. *Cancer Facts & Figures,* Atlanta, 2014.

2. L. Brannon-Peppas and J. O. Blanchette, *Adv Drug Deliv Rev.*, 2004, **56**, 1649-1659.

3. N. Kolishetti, S. Dhar, P. M. Valencia, L. Q. Lin, R. Karnik, S. J. Lippard, R. Langer and O. C. Farokhzad, *PNAS*, 2010, **107**, 17939- 17944.

4. G. Pasut, F. Greco, A. Mero, R. Mendichi, C. Fante, R. J. Green and F. M. Veronese, *J. Med. Chem.*, 2009, **52**, 6499- 6502.

5. E. R. Gillies and M. J. Frechet, *Drug Discov. Today*, 2005, **10**, 35-43.

6. R. Duncan, *Pharm Sci Technolo Today*, 1999, **2**, 441-449.

7. A. M. Caminade and C. O.Turrin, *J. Mat. Chem. B,* 2014, **00**, 1-12.

8. C. C. Lee, J. A. MacKay, J. M. J Frechet and F. C. Szoka, *Nat. Biotechnol.,* 2005, **23**, 1517-1526.

9. N. Q. Tran, C. K. Nguyen and T. P. Nguyen, *Adv. Nat. Sci.: Nanosci. Nanotechnol.*, 2013, **4**, 045013.

10. M. Mei, Y. Ren, X. Zhou, X. B. Yuan, F. Li, L. H. Jiang, C. S. Kang and Z. Yao, *J Appl Polym Sci.,* 2009, **114**, 3760-3766.

11. M. Zhang , R. Guo , M. Keri , I. Banyai , Y. Zheng , M. Cao , X. Cao and X. Shi, *J Phys Chem B.*, 2014, **118**, 1696-1706.

12. H. Liao, H. Liu, Y. Li, M. Zhang, H. Tomas, M. Shen and X. Shi, *J. Appl. Polym. Sci.,* 2014, **131**, 40358.

13. E. N. Cline, M. H. Li, S. K. Choi, J. F. Herbstman, N. Kaul, E. Meyhofer, G. Skiniotis, J. R. Baker, R. G. Larson and N. G. Walter, *Biomacromolecules*, 2013, **14**, 654-664.

14. H. M. Teow, Z. Zhou, M. Najlahb, S. R. Yusof, N. J. Abbott and A. D'Emanuelea, *Int J Pharm.,* 2013, **441**, 701-711.

15. A. Abderrezak, P. Bourassa, J. S. Mandeville, R. Sedaghat-Herati and H. A. Tajmir-Riahi, *PLoS One.,* 2012, **7**, e33102.

16. M. M. Yallapu, M. C. Ebeling, N. Chauhan, M. Jaggi and S. C. Chauhan, *Int J Nanomedicine.,* 2011, **6**, 2779-2790.

17. U. Gupta, H. B. Agashe, A. Asthana and N. K. Jain, *Biomacromolecules,* 2006, **7**, 649-658.

18. X. Yuan, S. Wen, M. Shena and X. Shi, *Anal. Methods,* 2013, **5**, 5486-5492.

19. X. Shi, K. Sun and J. R. Baker Jr, *J Phys Chem C Nanomater Interfaces.,* 2009, **112**, 8251-8258.

20. X. Shi, I. Lee and J. R. Baker Jr, *J. Mater. Chem.,* 2008, **18**, 586-593.

21. H. Wang, L. Zheng, C. Peng, M. Shen, X. Shi and G. Zhang, *Biomaterials*., 2013, **34**, 470-480.

22. H. Liu, H. Wang, R. Guo, X. Cao, J. Zhao, Y. Luo, M. Shen, G. Zhang and X. Shi, *Polym. Chem*., 2010, **1**, 1677-1683.

23. H. Liu, M. Shen, J. Zhao, J. Zhu, T. Xiao, X. Cao, G. Zhang and X. Shi, *Analyst,* 2013, **138**, 1979-1987.

24. A. R. Gliga, S. Skoglund, I. O. Wallinder, B. Fadeel and H. L. Karlsson, *Part Fibre Toxicol.,* 2014, **11**, 11.

25. P. Sanpui, A. Chattopadhyay and S. S. Ghosh, *ACS Appl. Mater. Interfaces,* 2011, **3**, 218-228.

26. S. Sharma, S. Chockalingam, P. Sanpui, A. Chattopadhyay and S. S. Ghosh, *Adv Healthc Mater.,* 2014, **3**, 106.

27. P. V. AshaRani , G. Low Kah Mun , M. P. Hande and S. Valiyaveettil , *ACS Nano,* 2009, **3**, 279-290.

28. P. Gopinath, S. K. Gogoi, P. Sanpui, A. Paul, A. Chattopadhyay and S. S. Ghosh, *Colloids Surf. B,* 2010, **77**, 240-245.

29. W. Liu, X. Li, Y. S. Wong, W. Zheng , Y. Zhang , W. Cao and T. Chen, *ACS Nano.,* 2012, **6**, 6578-6591.

30. G. W. Visser, G. C. Gorree, G. J. Peters and J. D. Herscheid, *Cancer Chemother. Pharmacol.,* 1990, **26**, 205-209.

31. S. U. Kumar, I. Matai, P. Dubey, B. Bhushan, A. Sachdev and P. Gopinath, *RSC Adv.,* 2014, **4**, 38263.

32. T. J. Lynch Jr., F. Kass, L. A. Kalish, A. D. Elias, G. Strauss, L. N. Shulman, D. J. Sugarbaker, A. Skarin and E. Frei, *Cancer.*, 1993, **71**, 2953-2957.

33. P. Gopinath, S. K. Gogoi, A. Chattopadhyay and S. S. Ghosh, *Nanotechnology*, 2008, **19**, 075104.

34. D. Liu, H. Hu, J. Zhang, X. Zhao, X. Tang and D. Chen, *Chem. Pharm. Bull.,* 2011*, **59**, 63-71.

35. R. J. Tallarida, *J. Pharmacol. Exp. Ther.,* 2001, **298**, 865-872.

36. Chou, *Pharmacol Rev.,* 2006, **58**, 621-681.

37. A. Buczkowski, P. Urbaniak and B. Palecz*, Int J Pharm*., 2012, **428**, 178– 182.

38. I. Matai, A. Sachdev, P. Dubey, S. U. Kumar, B. Bhushan and P. Gopinath, *Colloids Surf. B,* 2014, **115**, 359-367.

39. A. Buczkowski, H. Piekarski and B. Palecz, *J. Mol. Liq.,* 2012, **173***, 8-12.

40. H. H. Vargas, E. Ballestar, P. C. Saez, C.V. Kobbe, I. B. Rodriguez, M. Esteller and G. M. Bueno, J. Palacios, *Int. J. Cancer.,* 2006, **119**, 1164-1175.

41. Y. H. Lee, F. Y. Cheng, H. W. Chiu, J. C. Tsai, C. Y. Fang, C. W. Chen and Y. J. Wang, *Biomaterials,* 2014, **35***, 4706-4715.

42. P. Chairuangkitti, S. Lawanprasert, S. Roytrakul, S. Aueviriyavit, D. Phummiratch, K. Kulthong, P. Chanvorachote and R. Maniratanachote, *Toxicol In Vitro.,* 2013, **27**, 330-338.

43. S. Rello , J. C. Stockert , V. Moreno, A. Gámez , M. Pacheco , A. Juarranz , M. Canˇete and A. Villanueva, *Apoptosis,* 2005, **10**, 201-208.

44. J. J. Cohen, R. C. Duke, V. A. Fadok and K. S. Sellins, *Annu. Rev. Immunol.,* 1992, **10**, 267-293.

45. S. J. Martin and D. R. Green, *Crit. Rev. Oncol./Hematol.*, 1995, **18**, 137-153.

46. A. H. Wyllie, J. F. R. Kerr and A. R. Currie. *Int. Rev. Cytol.,* 1980, **68**, 251-306.

47. S. Allen, J. Sotos, M. J. Sylte and C. J. Czuprynski, *Clin. Diagn. Lab. Immunol.,* 2001, **8**, 460-464.

48. M. Cheng, B. He, T. Wan, W. Zhu, J. Han, B. Zha, H. Chen, F. Yang, Q. Li, W. Wang, H. Xu and T. Ye, *PLoS One*., 2012, **7**, 47115.

49. D. T. Chao and S. J. Korsmeyer, *Annu. Rev. Immunol.,* 1998, **16**, 395-419.

50. E. H. Yang, J. Zha, J. Jockel, L. B. Boise, C. B. Thompson and S. J. Korsmeyer, *Cell,* 1995, **80**, 285-291.

51. K. G. Wolter, Y. Hsu, C. L. Smith, A. Nechushtan, X. Xi and R. J. J. Youle, *Cell Biol.,* 1997, **139**, 1281-1292.

52. X. Liu, C. N. Kim, J. Yang, R. Jemmerson and X. Wang, *Cell,* 1996, **86**, 147-157.

53. M. O. Hengartner, *Nature,* 2000, **407**, 770-776.

54. Y.-H. Hsin , C.-F. Chen, S. Huang, T.-S. Shih, P.-S. Lai and P. J. Chueh , *Toxicol. Lett.,* 2008, **179**, 130-139.
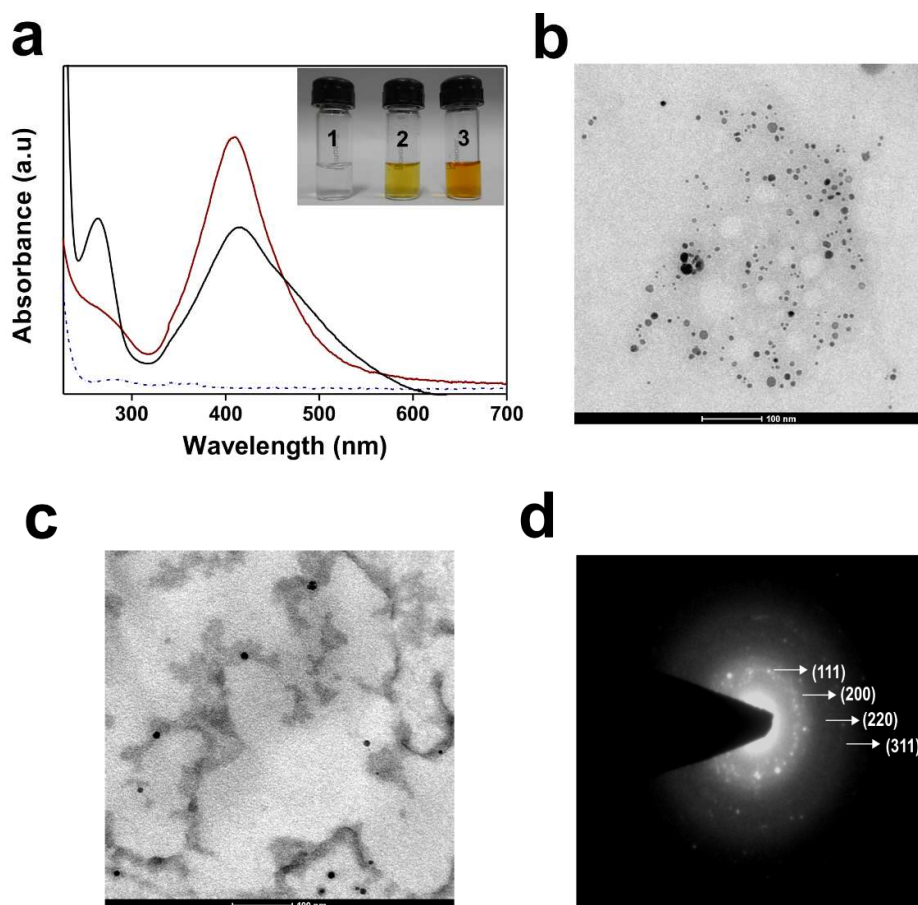
Main Figures

Figure 1. a) UV-vis spectra and corresponding photographs of G5 PAMAM.NH$_2$ (blue dotted line, 1), DsAgNPs (red line, 2) and 5-FU@DsAgNCs (black line, 3). Representative TEM images of (b) DsAgNPs and (c) 5-FU@DsAgNCs (Scale bar: 100 nm). c) Corresponding SAED pattern of 5-FU@DsAgNCs.
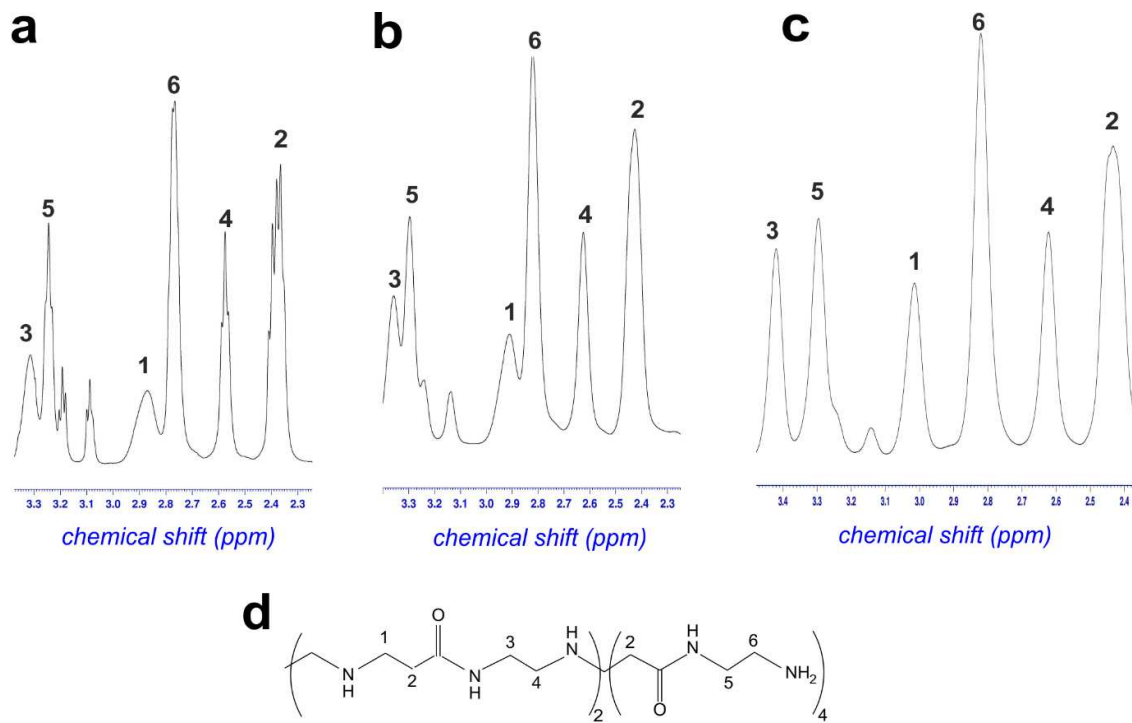
Figure 2. ^{1}H NMR spectra of a) G5 PAMAM.NH$_2$, b) DsAgNPs and c) 5-FU@DsAgNCs. A schematic of the dendrimer structure used in NMR experiments is depicted in (d).
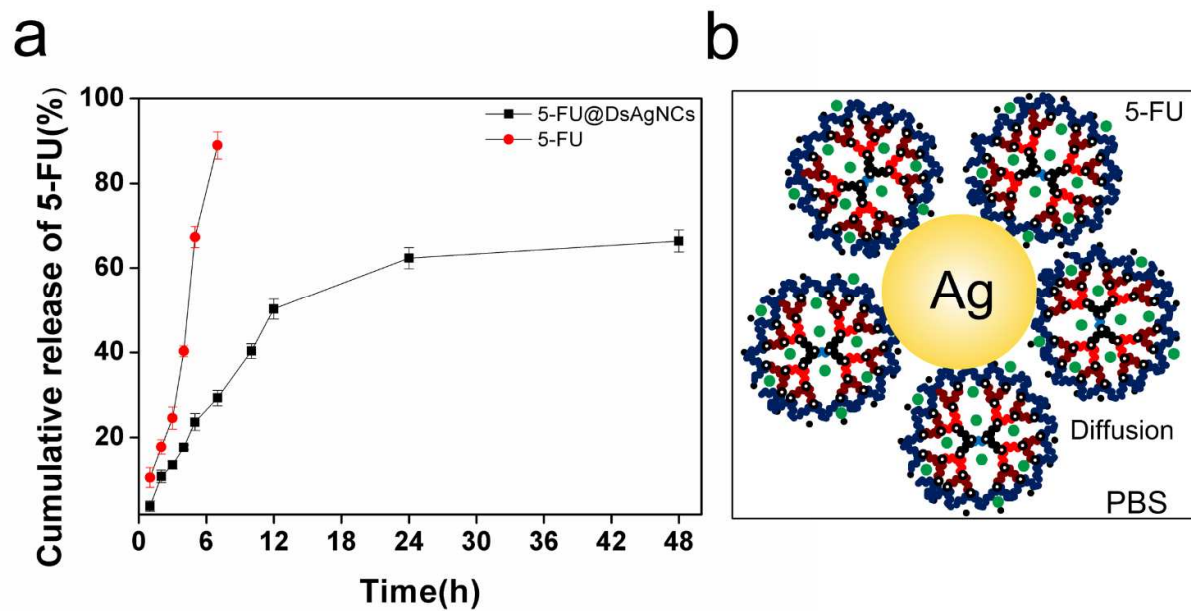
Figure 3. a) Cumulative release of 5-FU from 5-FU@DsAgNCs in PBS (pH = 7.4) (b) Schematic representation of 5-FU release from 5-FU@DsAgNCs.
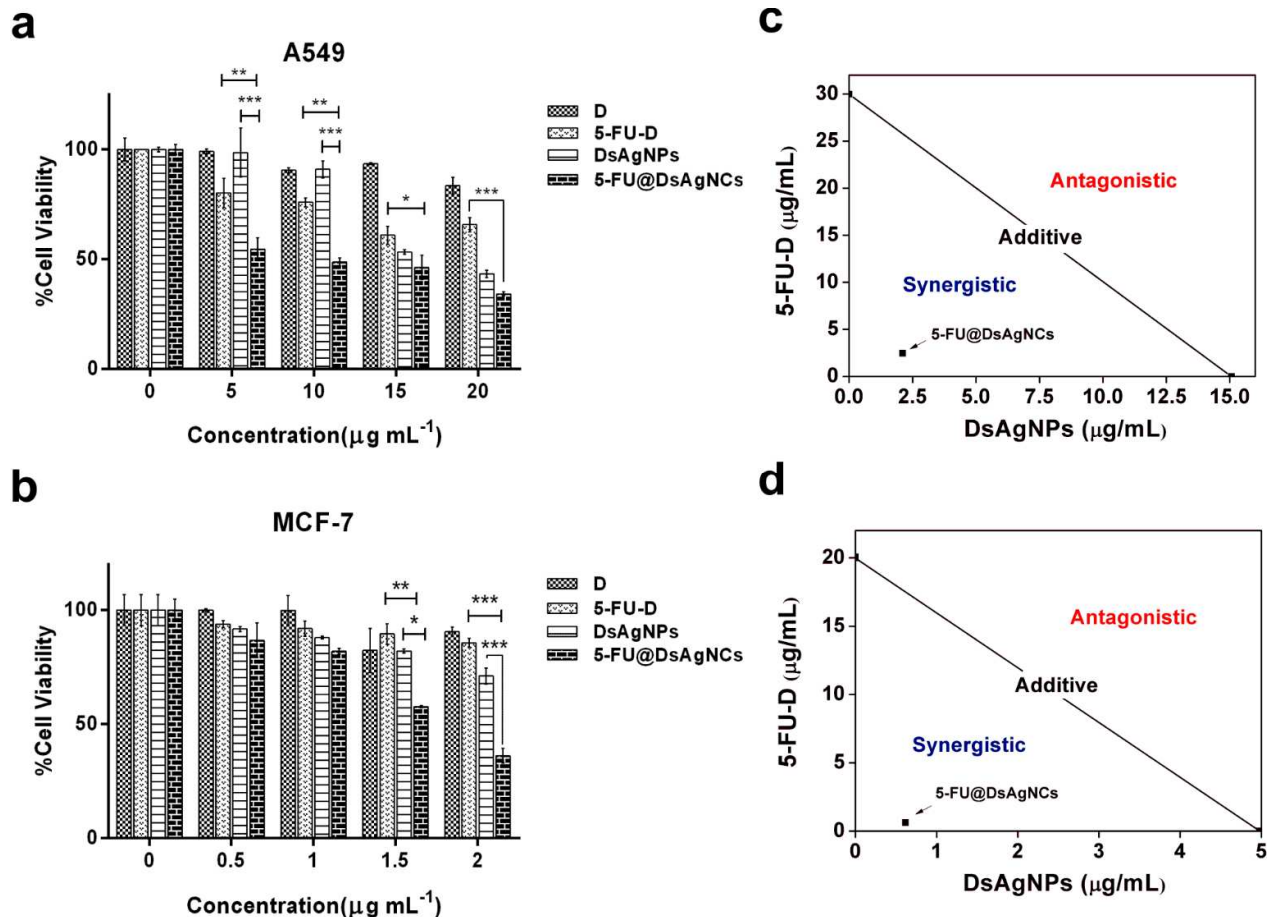
Figure 4. Cell viability of (a) A549 and (b) MCF-7 cells as calculated from the MTT assay. The cells were treated with blank PAMAM dendrimer (D), 5-FU-D, DsAgNPs and 5-FU@DsAgNCs (Concentration of Ag was equivalent to 5-FU in 5-FU@DsAgNCs sample). The values are represented as mean ± S.E.M (n =3).Two-way ANOVA with Bonferroni correction was done to determine multiple comparisons between the groups. Statistical significance between different samples is denoted by * ($p < 0.05$), ** ($p < 0.005$), and *** ($p < 0.001$). Synergy analysis between 5-FU and DsAgNPs as constituents of 5-FU@DsAgNCs and corresponding isobolograms of A549 and MCF-7 are shown in (c) and (d), respectively.
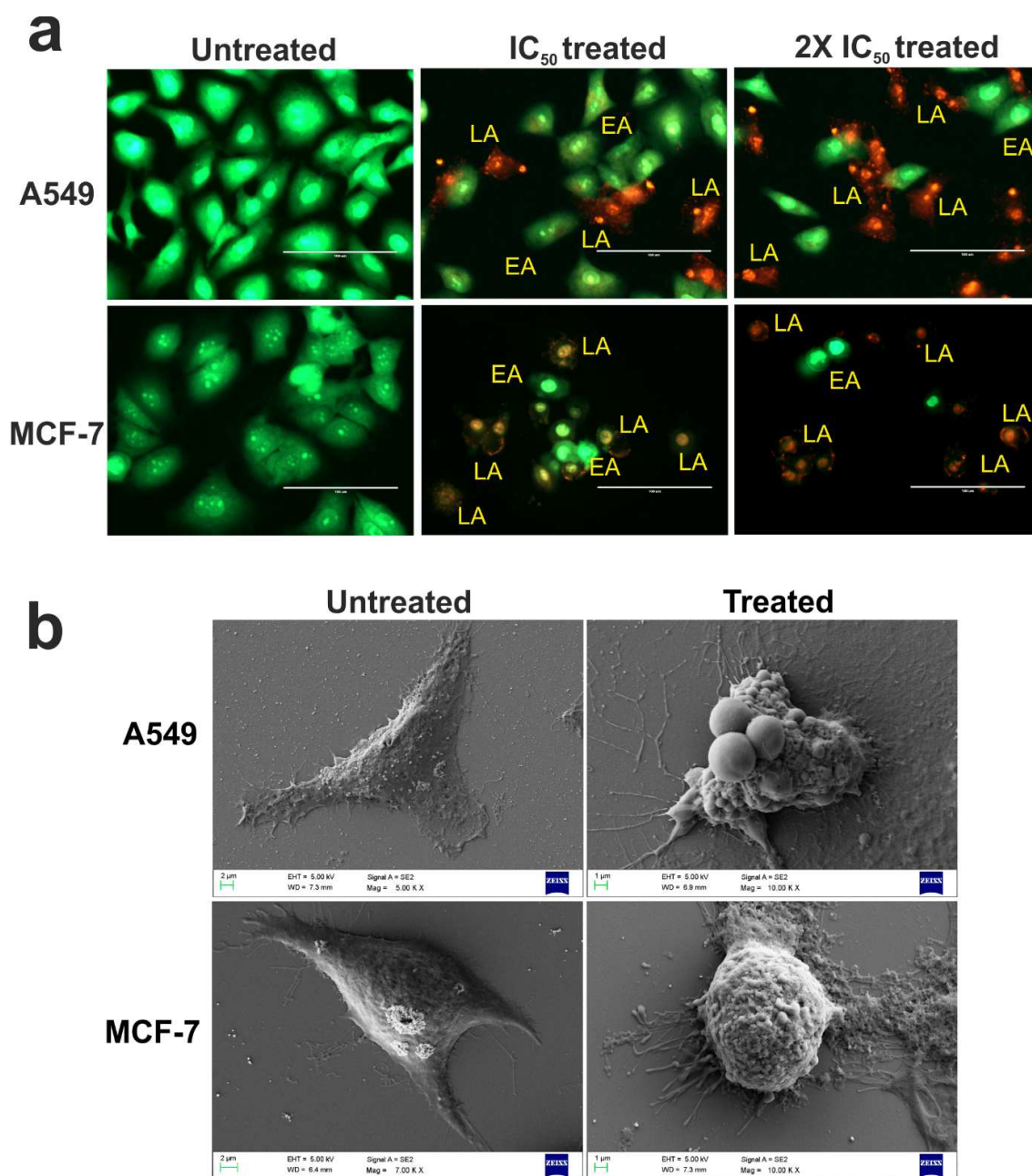
Figure 5. a) Representative AO/EB dual staining images of untreated, IC_{50} and 2X IC_{50} 5-FU@DsAgNC treated A549 and MCF-7 cells. EA and LA represent early apoptotic and late apoptotic cells, respectively. Scale bar: 100 μm. b) FE-SEM images of untreated and IC_{50} 5-FU@DsAgNC treated A549 and MCF-7 cells, respectively.
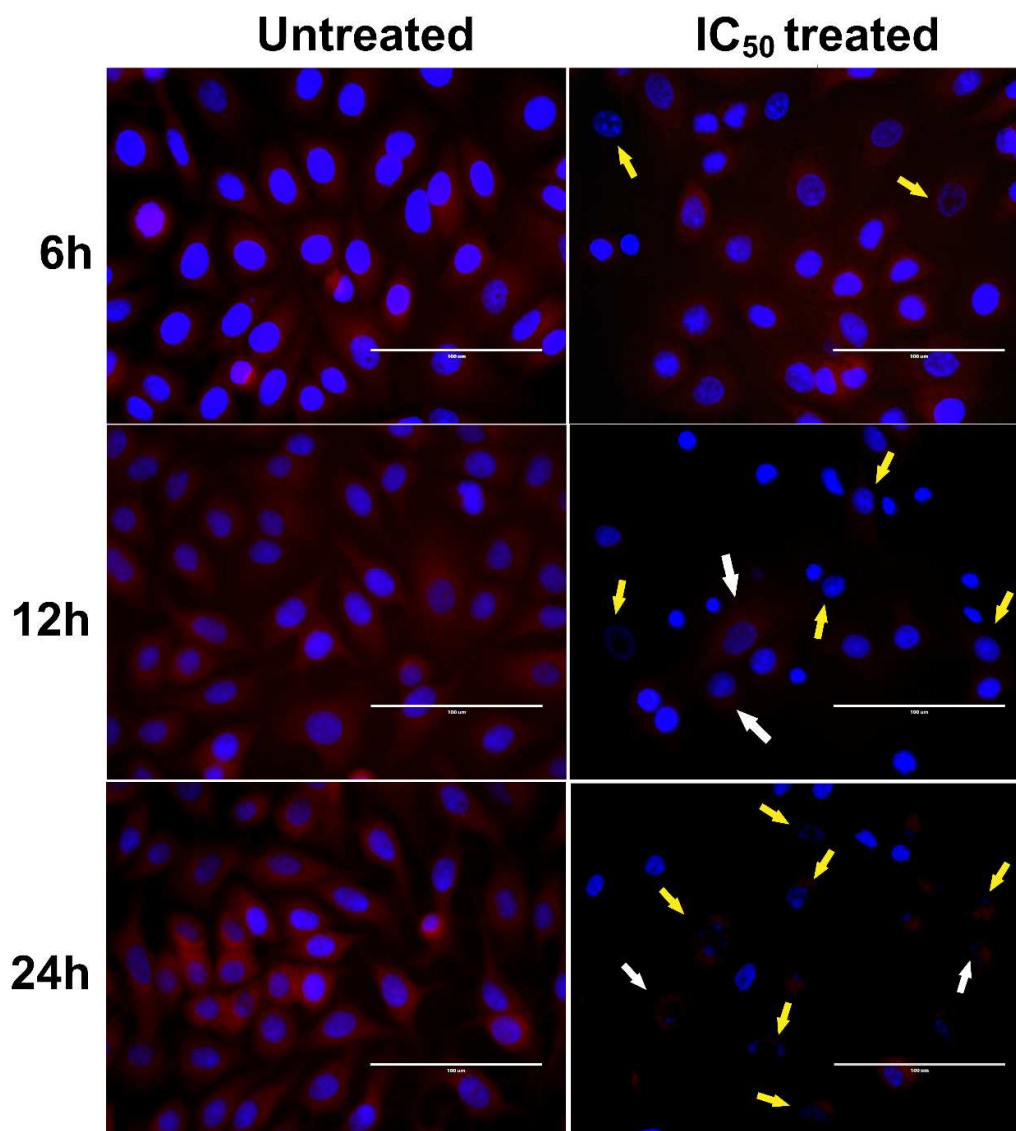
Figure 6. Time-dependent overlay images of untreated and 5-FU@DsAgNC (IC$_{50}$) treated MCF-7 cells stained with Hoechst 33342 (blue) and co-stained with rhodamine B (red). Yellow arrows indicate chromatin condensation (dark spots) and white arrows point towards cytoskeleton compaction. Scale bar: 100 μm.
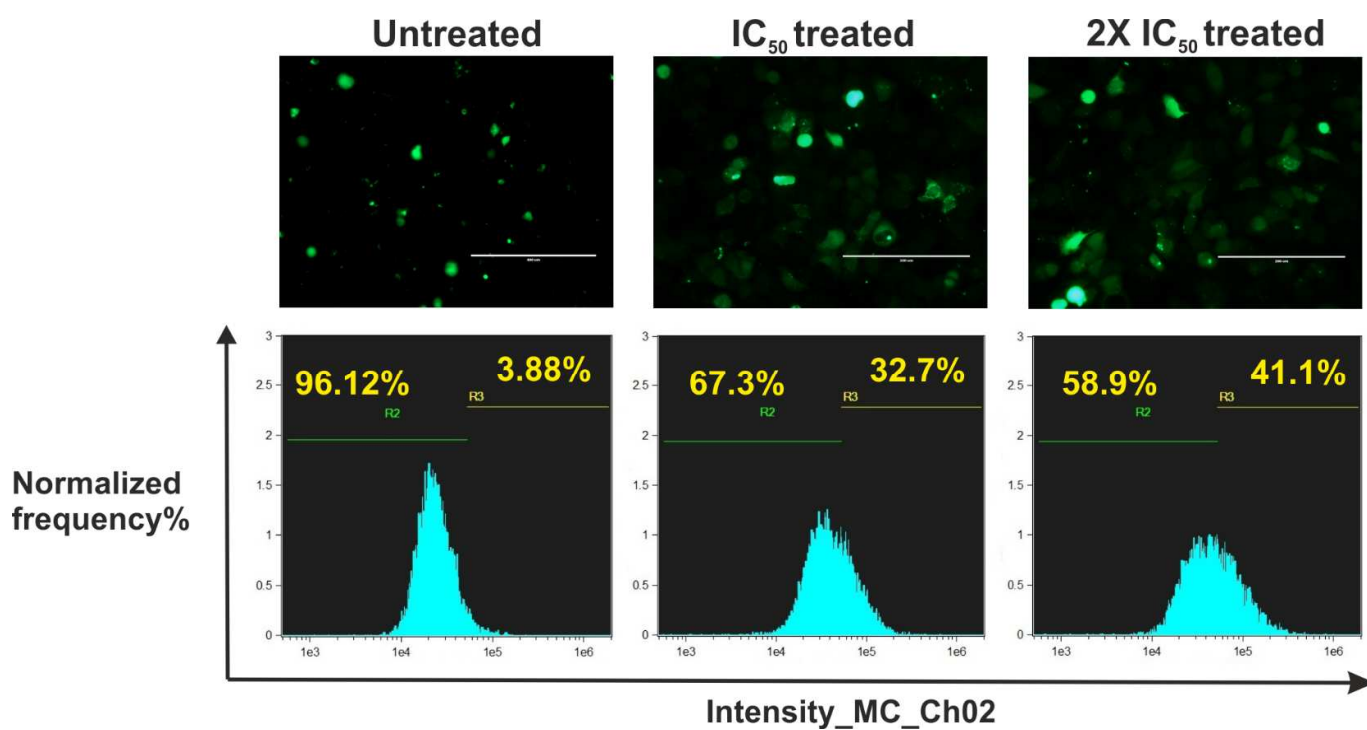
Figure 7. Microscopic and flow cytometric analysis of ROS production in MCF-7 cells treated with different concentrations of 5-FU@DsAgNCs. Upper panel: Green DCF fluorescence indicates intracellular ROS generation. Scale bar: 100 μm. Lower panel: Corresponding flow cytometric quantitation.
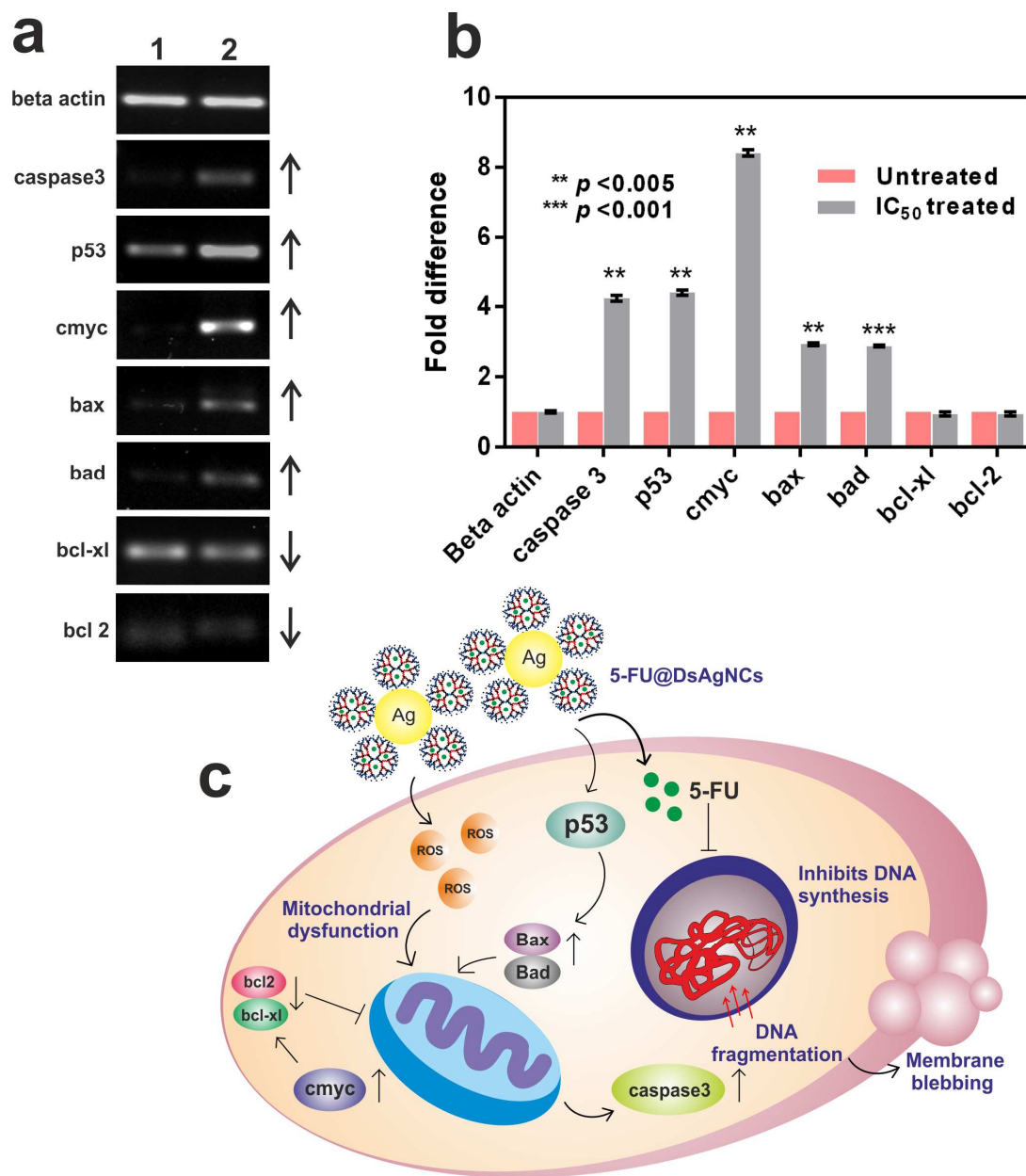
Figure 8. a) Semi-quantitative RT-PCR analysis of apoptotic signalling genes and their representative images. Lane 1 and 2: Untreated and 1.5 μg mL^{-1} 5-FU@DsAgNC (IC$_{50}$) treated MCF-7 cells. b) Fold difference in gene expression represented as mean ± S.E.M of individual experiments (n =3). c) Schematic representation of progressive apoptotic events involved in 5-FU@DsAgNCs treatment.